Eng. & Tech. Journal, Vol.28, No.12, 2010

Numerical and Experimental Analyses for Effect of Welding Currents on Cooling Rates in (M MAW) Process

Dr.Muna K. Abbass*, Dr. Jalal M. Jalil & Dr. Abbas Sh. Alwan***

Received on: 7/6/2009
Accepted on:7/1/2010

Abstract

In this study, Manual Metal Arc Welding (MMAW) is carried out for low carbon steel (AISI 1015) with using electrode (E7018). Direct current straight polarity (DCSP) with the joint geometry of single -V- butt joint and weld one pass are used for plate of thickness 8mm. experimentally, obtained temperature distribution in fusion zone which is measured by insert the thermocouple in weld metal. Cooling rates are determined for the fusion zone at different welding currents (100, 120 and 140) Amp with constant welding speed at 3.2mm/s. Numerical analysis by using the Control Volume Method (CVM), applied to three-dimensional heat transfer model to determine the cooling rate in fusion zone. Cooling rates models are helping in prediction the microstructure (phases, grain size and volume fraction) and microhardness distribution in weld metal and heat affected zone. The comparison of cooling curves between numerical and experimental work have a good agreement, so that deviation was in range (6% - 21%) which is confirming the capability and reliability of the proposed numerical heat transfer model in manual metal arc welding. The best result for cooling rates when applying mathematical model is at welding current 140Amp.

Keywords: Manual Metal Arc Welding, Cooling Curves, Finite Volume Method.

التحليلات العددية والعملية لتاثير تيارات اللحام على معدلات التبريد بطريقة لحام القوس الكهربائي اليدوي

الخلاصه

في هذه الدراسه تم لحام صفائح من الفولاذ منخفض الكربون نوع (AISI 1015) بطريقة لحام القوس الكهربائي المعدني (MMAW) باستخدام قطب لحام نوع (E7018) وقطبية مباشرة (DCSP) على شكل وصلات تناكبية مفردة (Single –V) وبتمريرة لصفيحة ذات سمك 8 mm. وتم عمليا قياس درجة الحراره في منطقة الانصهار (معدن اللحام) بوضع مزدوج حراري في (معدن اللحام) وبعد ذلك تم رسم منحنيات التبريد مع اختلاف تيارات اللحام (100, 120, 140) أمبير عند سرعة لحام ثابته (3.2mm/s). اما الدراسة النظرية فقد تضمنت التحليلات العددية لايجاد معدلات التبريد باستخدام طريقة الحجم المحدود والتي طبقت لانتقال الحرارة الثلاثي الابعاد. وقد ساهمت معدلات التبريد النظرية بشكل فعال في التنبؤ عن البنية المجهرية (الاطوار, الحجم الحبيبي, والكسر الحجمي) وكذلك توزيع الصلادة الدقيقة في معدن اللحام والمنطقة المتاثرة بالحرارة. ولغرض التحقق من صحة النتائج العددية المستحصلة من البرنامج الحاسوبي تم اجراء المقارنة مع النتائج العملية المستحصلة من التجارب المختبرية حيث كانت النتائج متوافقة بشكل جيد وكان مقدار التقارب

*Production & Metallurgy Engineering Department,University of Technology/Baghdad
**Electromechanical Engineering Department, University of Technology/Baghdad

يتراوح (6%- 21%) كما تم الحصول على افضل نتيجة لمعدلات التبريد عند تطبيق أ لموديـــل الرياضي هي عند تيار لحام (140) أمبير.

Introduction

Manual Metal Arc Welding (MMAW) process uses the filler metal as a consumable electrode through the center of the weldement. In this case, when the electrode comes close to the workpiece, an arc is struck between the filler metal and the workpiece, and the filler metal melts and joints two plates by filling metal droplet simultaneously in V-groove of plates. In the present work the three - dimensional model main effort will be used the application of control volume method (CVM) in the modelling of rapid solidification processes. This method is a suitable for problems where the phase change occurs and moving the interface at a high temperature [1]. **Svensson et al [1] (1986)** studied experimentally determined cooling curve for the fusion zone of manual metal arc welding for three-dimensional heat flow. The welding was carried out in the flat position, with plate thickness being 20mm, plate length was 330mm and 4mm diameter electrode (ESAB OK 48.00). They found that the microstructure of welds is complex, consisting of allotriomorphic ferrite (α), Widmanstatten ferrite (α_w) and acicular ferrite (α_a). **Murugan et al [2] (2001)** investigated residual stresses and temperature distribution of AISI 304 stainless steel and low carbon steel welds. Thy used manual metal arc welding process to weld plate of thickness 6, 8 and 12mm. They found that the temperature range (250 °C and 700 °C) is important with respect to formation of residual stresses in both of stainless steel and low carbon steel welds. **Cristiene et al [3] (2002)** studied the simulation annealing inverse technique to estimate the temperature history in gas tungsten arc welding (GTAW) workpiece. The test plate was made of stainless steel AISI 304, with dimensions (0.2 m × 0.05 m × 0.004 m). In this case, a two-dimensional model with moving heat source is used, the component of the heat flux input that goes into the workpiece. The results indicate a good agreement between the predicted and the measured temperature. **Moneer et al [4] (2006)** studied the evaluation and simulation of angular distortion in welding joints. They used shielded metal arc welding (SMAW) process to weld plates of low carbon steel type (A-283-C).Temperature distributions are obtained using finite difference method. In this work transient heat conduction equation is solved using FDM. The most important results are the value of angular distortion increased with the increased current, angular distortion decrease with the increased thickness of plates and the square butt joints have fewer distortions than single-v joints. The aim of this work is to study the effect of welding current on cooling rates, microstructure and microhardness of welded joints, experimentally and numerically by using finite volume method to a three dimensional heat transfer model. A comparison between the experimental and the numerical analyses results.

Experimental Work

1- The Base Metal

Low carbon steel (AISI 10150) is used in this work it is widely used in pipes and large storage tank structures and other applications. The chemical composition of low carbon steel is shown in **Table 1.** The mechanical properties of AISI-1015 are shown in **Table 2 [5].**

2- Plate Preparation

Low carbon steel plates with dimensions of (100 mm ×50 mm×8 mm) were used in manual arc welding process. The plates were prepared by milling machine from both surfaces and V- single butt joint is designed by machining the specimen to angle (30^o) from both sides as shown in **Figure 1.**

3- Welding Electrodes

The chemical composition of the welding electrode, which is used in this work, is shown in **Table 3.** According to AWS (A5.1) **[5]**, arc welding specification of electrodes classification, the mechanical properties of electrode (E7018) are shown in **Table 4.**

4- Welding procedure

Manual metal arc welding (MMAW) Process is carried out using electrode of diameter 3.2mm. The welding machine used in this work was type (LHI825), Ideal arc DC-600-Lincoln Company-Sweden. Three welding currents are shown in **Tables 5.** Butt V-single joint is designed with one pass for specimen thickness (8mm) and fixing the thermocouples type (S) in the fusion zone which is connected with readers type (TE9-R10). Recording the values of welding temperatures during each welding process by using video camera (7.2 Mega pixels) with sensitivity (ISO 1000). The welding time is recorded using stop watch.

Tests and Measurements

1- Temperature measurement was carried out by inserting the thermocouples type (S) in the fusion zone (weld metal) and the readings were recorded by video camera. Cooling curves were obtained by drawing the relationship between fusion zone temperature and time.

2- Microstructure test by using optical microscopy, connected with computer.

3- Microhardness test by using digital microhardness tester type (QV-100-Qualitest company-Japan).

4- Grain size and volume fraction were measured by using (J-Image) and (S-Image) programs respectively.

5- X-Ray Diffraction instrument type XRD-6000-Shimadzu, Japan is used to determine the phases obtained in weld metal joints. To determine inter planer spacing distance (d) Bragg law must be used; $n\lambda = 2d\sin\theta$.

Numerical Method

In the present work, the numerical method is Control Volume Method (CVM) which employed heat transfer and predict of phase change with moving interface. This method is base on the cell-centered finite volume (FV) method and conservation principle i.e. energy balance is expressed for the control volume method. The computer flow chart considers the numerical solution by (CV) method program of manual arc welding process as shown in **Figure 3.**

1- Assumptions

The three - dimensional model for simulation of welding process of the present work used the following assumptions are

1- The convection and radiation heat transfer were neglected.

2- The fluid movement within the welding joint during melting process was neglected.

3- The energy from the arc welding heat source is applied at a uniform rate.

4- The weld metal droplet (molten) is moving with a constant speed.

5- All the plate boundaries were assumed to be insulated.

6- Symmetry between right and left half of the welded plate was assumed.

7- The heat transfer from the filler metal droplets is taken into account using time-volumetric heat source and filling it instantaneously.

8- The weld physical properties data used in this analysis are summarized in **Table 6 [6],** dependent on the material type.

2- Initial and Boundary Conditions

Initial conditions are required only when dealing with transient heat transfer (weld metal) problems in which temperature of material changes with time (**Figure 4**). The boundary conditions used in the welding boundary conditions are:-

1-Top surface; the weld top surface is assumed to be flat and insulated. The welding velocity component along the X, and Y directions equal to zero, while the velocity of welding along Z is varied with welding parameters.

2- Symmetrical surface; the boundary conditions are defined as zero flux across the symmetrical surface.
3- Other surfaces; all other surfaces are insulated.
4- The initial preheat temperatures before welding is 100°C.

3- Governing equations

For most of rapid solidification, there is no clear boundary between the liquid and solid; for this case the enthalpy is more appropriate **[6].** A three-dimensional volumetric heat source model is the conservation of energy equation in the enthalpy (E) method is considered in term of enthalpy instead of temperature. The governing equations are based directly on the model **[7]**:-

$$\frac{\partial(rE)}{\partial t}=\frac{\partial^2(\Gamma E)}{\partial X^2}+\frac{\partial^2(\Gamma E)}{\partial Y^2}+\frac{\partial^2(\Gamma E)}{\partial Z^2}+P \quad \text{....(1)}$$

$$P=\frac{\partial^2 S}{\partial X^2}+\frac{\partial^2 S}{\partial Y^2}+\frac{\partial^2 S}{\partial Z^2}$$

$$\Gamma=\Gamma(E), S=S(E)$$

The energy equation has been transformed into a non-linear equation with a single dependent variable E. The non-linearity of the phase –change problem is evident in the above equation.

In the liquid region, equation (1) reduces to the normal linear energy equation **[7].**

$$\frac{\partial(r_L E)}{\partial t}=\frac{\partial}{\partial X}\left(k_L\frac{\partial T}{\partial X}\right)+\frac{\partial}{\partial Y}\left(k_L\frac{\partial T}{\partial Y}\right)+\frac{\partial}{\partial Z}\left(k_L\frac{\partial T}{\partial Z}\right) \quad \text{....(2)}$$

Also, in the solid region equation (1) reduces to

$$\frac{\partial(r_S E)}{\partial t}=\frac{\partial}{\partial X}\left(k_S\frac{\partial T}{\partial X}\right)+\frac{\partial}{\partial Y}\left(k_S\frac{\partial T}{\partial Y}\right)+\frac{\partial}{\partial Z}\left(k_S\frac{\partial T}{\partial Z}\right) \quad \text{...(3)}$$

4- Numerical Solution of Weld Metal Deposits

The welding currents are affected on cooling cycles result from the amount of weld metal deposits. The three- dimensional numerical heat transfer from the arc welding, additional heat from the metal droplets. The weld metal is moving along V-joint with the electrode is melting and deposits droplet spontaneously in weld joint. The calculation of weld volume deposits per second and filling area of weld metal with different welding current. The following equation depends on sensible heat and latent heat is **[8]**

$$\mathbf{V^{\circ} = I \times V \times \eta / \rho\, [C_p\, (T_L - T_S) + h]}\ \mathrm{mm^3/s} \quad \ldots(4)$$

Where:
$\mathbf{V^{\circ}}$ is the metal volume deposit per second, I is weld current (A), **V** is voltage (volt), η is arc welding efficiency = 0.70, ρ: density = (7860 kg/m^3), C_p is specific heat (450J/kg. $^{\circ}$C), ΔT is temperature difference = (T_L- T_S) and h is latent heat =2.7×10^5 J/ kg.

The filling area of weld metal deposits, with different welding currents are calculated by,
Deposited Area=$(\mathbf{V^{\circ}} / S)\ mm^2$ ….(5)

Where; S is travel welding speed (mm/s)

Results and discussion

1- Effect of welding current on cooling rate

The results obtained from the experimental work, increasing welding current leads to increase heat input and decrease cooling rates as shown **Figures 5.** This result is in good agreement with the result of **Andrea Lund back [9].**

2- Effect of the Welding Current on Microstructure

The grain boundary ferrite increases when the heat input is increased in the fusion zone region to a temperature well above 910°C and this allowing austenite grains to grow. The high cooling rate and large grain size encourage the ferrite to form side plates from the grain boundaries called Widmanstatten ferrite. This result is in good agreement with result of Yang. Et al [`10]. Figure 6a, shows the weld microstructure which is consisted of fine acicular ferrite (AF) and widmanstatten Ferrite (WF). An increase in the welding currents leads to increasing the veins of grain boundary ferrite on prior austenite grain in fusion zone as shown in **Figure 6b, c**. The results of X- ray is explained the type of phases with different welding current as shown in **Figure 7**.

3- Effects of Welding Current on the Microhardness

Welding current is the most important factor that effecting on microhardness. The hardness drops with increasing the welding current or heat input which increases the width of weld metal and heat affected regions as shown in **Figure 8.** An increasing welding current lead to decreasing cooling rates and that effect is decreased the microhardness of welded joint.

4- Simulation Results

The effect of the welding current at constant welding speed on cooling curves, decreases cooling rate with an increase in welding current as shown in **Figure 2.** These results are in agreement with results of **Gareth, et al [12]** and **Chol, and J.Mazumder [13]**. **Figure 9** and **10** shows the temperature history at x=0 plane with different welding current and decrease weld metal deposited with decreased welding current.

5- Analysis of Cooling Curves

Equations 6, 7 and 8 represent the models of cooling rate at welding speed 3.2 mm/s, preheat temperatures 100°C and welding current (100, 120 and 140 Amp) respectively. An increase welding current leads to decrease cooling rates. The data was fitted as shown in **Figure 2.**

Using computer program the curves equations are:

$$dT/dt = - 113.05 * t^{(-1.19)} \quad \text{….(6)}$$

$$dT/dt = - 93.38 * t^{(-1.14)} \quad \text{…(7)}$$

$$dT/dt = - 77.66 * t^{(-1.11)} \quad \text{….(8)}$$

Where; dT/dt is cooling rate and (t) is the time (second)

6- Prediction of Microstructure

The effects of welding current on cooling curves, as the welding current is a function of heat input. An increase welding current lead to decrease cooling rates which was represented by equations (6), (7) and (9). These equations are helping to predict the microstructure of weld metal (WM and (HAZ) regions as shown in **Figures 6.**

7- Prediction of Ferrite phase's volume fraction

The cooling rates are helping to predicting the volume fraction of phases in weld metal (WM) and heat affected zone (HAZ) as shown in **Table 7.**

8- Prediction of microhardness

Microhardness decreases with increasing welding current as result from decreasing cooling rates. **Table 8** shows the prediction of microhardness in weld metal and heat affected zones with various cooling rates models.

9- Prediction of grain size

The grain size increases with decreasing the cooling rate (increase welding current). These cooling rates help us prediction the grain size of weld metal and heat affected zone as shown in **Table 9.**

10- Prediction the width of weld metal and heat affected regions

The cooling rate models are helping to estimate the width of WM and HAZ regions depends on microhardness test. **Table 10** shows the prediction width of weld metal (WM) and heat affected zones (HAZ) with various welding currents.

11- Experimental verification

The Experimental results are matching with earlier numerical results. **Figure 11** shows the comparison between numerical and experimental results of cooling curves at different current. The deviation between numerical and experimental causes the different boundary conditions.

Conclusions

1- Increasing welding current (increase the heat input) leads to a reduction in cooling rate and an increasing the grain size of weld metal and heat affected zone. An increases welding current lead to increases the width of HAZ region and increases the volume fraction and decreases the microhardness.

2- Normalizing heat treatment has clear effect on grain size; it changes the original welded microstructure (columnar structure) to an equiaxial structure of weld metal.

3- The formation of microphase's acicular, wedmanstatten and polygonal ferrites (AF, WF, PF) in weld metal are affected by welding currents.

4- The mathematical model of (cooling rate) of welding current at constant welding speed (3.2 mm/s), welding current (140A) and preheat temperature (100°C) for plate thickness (8mm) is [$dT/dt = -77.66 * t^{(-1.11)}$].

5- Analysis of cooling rates with various welding currents helps to predict of microstructures and microhardness distribution of weld metal and heat affected zone.

6- The result which obtained was a good agreement between the predicted and the measured temperature**.**

References

[1**]** Svensson.L.E. B.Gretoft and H.K.D.H.Bhadeshi," An Analysis of Cooling Curves from the Fusion Zone of Steel Weld Deposits", Scandinavian Journal of Metallurgy 15 pp 97-103, (1986).

[2] Murugan , Sanjaik K.Rai , P.V.Kumar, and T.Jayakumar," Temperature Distribution and Residual Stresses due to Multipass Welding in Type 304 Stainless Steel and Low Carbon Steel Weld Pads", International Journal of Pressure Vessel and Piping78 pp 307-31(2001).

[3] Cristiene V.Goncalves and Gilmar Guimarae," Inverse Technique Applied in Welding; A theoretical and Experimental Approach", 4th International Conference on inverse problems in Engineering, Brazil, (2002).

[4] Moneer H.Al-Saady, Mudar A.Abdulsattar and Laith S.Al-Khafagy," Finite Difference Simulation of Low Carbon Steel Manual Arc Welding, International Conference on Modelling and Simulation", Turkey, 28-30, Paper No.A125 August, (2006).

[5] Richard S.Sabo, " The Production HandBook of Arc Welding", The Lincolin electric company, Cleveland, Ohio 44117, USA, 1999.

[6] Hattel.J.H and N.H.Pryds," Modeling Rapid Solidification with the Control Volume Method", Riso National Lab-, Denmark, pp 241-247, (2001).

[7]Yiding Cao , and Amir Faghri," A numerical Analysis of Stefan Problem for Generalized Multi-dimensional Phase –Change *Structures Using the Enthalpy Transformation Model*", International Journal of Heat and Mass Transfer, Vol. 32, No.7, pp 1289 **–** 1298, (1989).

[8]Kumar, and T.Debroy," Guaranteed fillet weld geometry from heat transfer model and multivariable optimization", International Journal of Heat and mass Transfer, pp 5793 **–** 5806, (2004).

[9]Andrea Lundback," *Finite Element Modelling and Simulation of Welding of Aerospace Component*", Department of Applied Physics and Mechanical Engineering, Lulea University of Technology, 27.Issn, pp 1402-1757, (2003).

[10]Yang. Z. and T.Debroy," *Modeling Macro-and Microstructures of Gas-Metal-Arc Welded HSLA-100 Steel*", Metallurgical and Materials Transactions, Vol. 30B, , PP 483-492, June (1999).

[11] Trindade Filho, A.S.Guimaraes and J.da payao Filho," Normalizing *Heat Treatment Effect on Low Alloy* Steel Welds

Metal", Vol. XXVI, No.1, pp 62-66. March, (2004),

[12] Gareth, A. Taylor, Michael and Koulis Pericleous," Finite Volume methods Applied to the Computational Modeling of Welding Phenomena", Second International Conference on CFD in the Mineral and Process Industries, Australia, 6-8 December (1999).

[13] Chol, and J.Mazumder, "Numerical and Experimental Analysis for Solidification and Residual Stress in the GMAW Process for AISI 304 Stainless Steel", Journal of Materials Science 37, pp 2143-2158, (2002).

[14] Salah Sabeh Abed–AL Kreem," Evaluation of Temperature Distribution and Fluid Flow in Fusion Welding Processes", PhD Thesis, Mechanical Engineering department, Engineering college of Baghdad, (2005).

Table (1) Chemical Composition of Low Carbon Steel (AISI-1015)

Element	C%	Si%	Mn%	P%	S%	Cr%	Mo%	Ni%	Cu%	Ti%	V%	Fe%
wt%	.163	.252	.442	.018	.047	.081	.02	.02	.053	.006	.01	Rem

Table (2) Mechanical Properties of Low Carbon Steel AISI-1015[5].

AISI - SAE, NO	Condition	Tensile strength (pa)	Yield strength (pa)	Elongation (%)
1015	Hot roll Cold roll	32148×10^3 365382×10^3	179244×10^3 303336×10^3	28 20

Table (3) Chemical Composition of Welding Electrode 7018 [13].

Element	C	Si	Mn	Cr	Ni	Mo	P	S	Cu	V	Ti	Fe%
Wt%	0.095	0.37	0.88	0.043	0.019	0.009	-	-	-	0.012	-	Rem

Table (4) AWS A5.1-69 Mechanical Properties of Arc Welding Electrode [5].

AWS Electrode	Tensile ,min strength(pa)	Yield, min strength(pa)	Elongation .in 2in. (%)	V-Notch Impact
E7018	496368×104	41364×104	22	20ft/lb-20°F

Table (5) Experimental welding conditions of manual metal arc welding (MMAW), with one pass, electrode E7018 of diameter (3.2 mm) and plate thickness (8mm).

Sample	Welding current (A)	Welding speed (mm/s)	Preheat temperature (°C)	Heat input (KJ/mm)
C1	100	3.2	100	0.48
C2	120	3.2	100	0.60
C3	140	3.2	100	0.74

Table (6) Physical Properties for deposition weld metal of electrode (E7018) [6].

Symbol	Property	Value	Unit
ρ_L	Liquid density	6980	kg /m³
ρ_S	Solid density	7860	kg /m³
k_L	Liquid thermal conductivity	31	W/m. K
k_S	Solid thermal conductivity	45	W/m.K
Cp_L	Liquid specific heat	450	J/kg. K
Cp_S	solid specific heat	450	J/kg. K
T_L	Liquids temperature	1500	˚C
T_S	Solids temperature	27	˚C
H	Latent heat	2.7×105	J/kg
T_m	Melting temperature	1483	˚C

Table (7) Prediction of ferrite volume fraction in weld metal and heat affected zones with various cooling rates models.

Welding Currents (Amp)	Cooling rate models	% Volume fraction		
		WM	HAZ Grain growth	HAZ Grain refinement
100	dT/dt = - 113.05 * t (-1.19)	0.42487	0.55637	0.432690.0.
120	dT/dt = - 93.38 * t (-1.14)	0.44256	0.45128	43328
140	dT/dt = - 77.66 * t (-1.11)	0.49486	0.46365	0.38834

Table (8) Prediction of microhardness in weld metal and heat affected zones with various cooling rates models.

Welding Currents (Amp)	Cooling rate models	Hardness of (WM) HV	Hardness of (HAZ) refinement HV
100 120 140	dT/dt = - 113.05 * t (-1.19) dT/dt = - 93.38 * t (-1.14) dT/dt = - 77.66 * t (-1.11)	220 210 190	235 220 210

Table (9) Prediction of grain size in weld metal and heat affected zones with various cooling rates models.

Welding Currents (Amp)	Cooling rate models	Grain size(µm)		
		WM at center	(HAZ) Grain growth	(HAZ) Grain refinement
100 120 140	dT/dt = - 113.05 * t (-1.19) dT/dt = - 93.38 * t (-1.14) dT/dt = - 77.66 * t (-1.11)	15.61 16.32 17.26	16.15 18.98 19.21	13.21 14.49 15.60

Table (10) Prediction of Weld Metal (WM) width and Heat Affected Zones (HAZ) width with various cooling rates models.

Welding Currents (Amp)	Cooling rate models	Width center of (WM) mm	Width of (HAZ) mm
100 120 140	dT/dt = - 113.05 * t (-1.19) dT/dt = - 93.38 * t (-1.14) dT/dt = - 77.66 * t (-1.11)	4 5 6	2 3 4

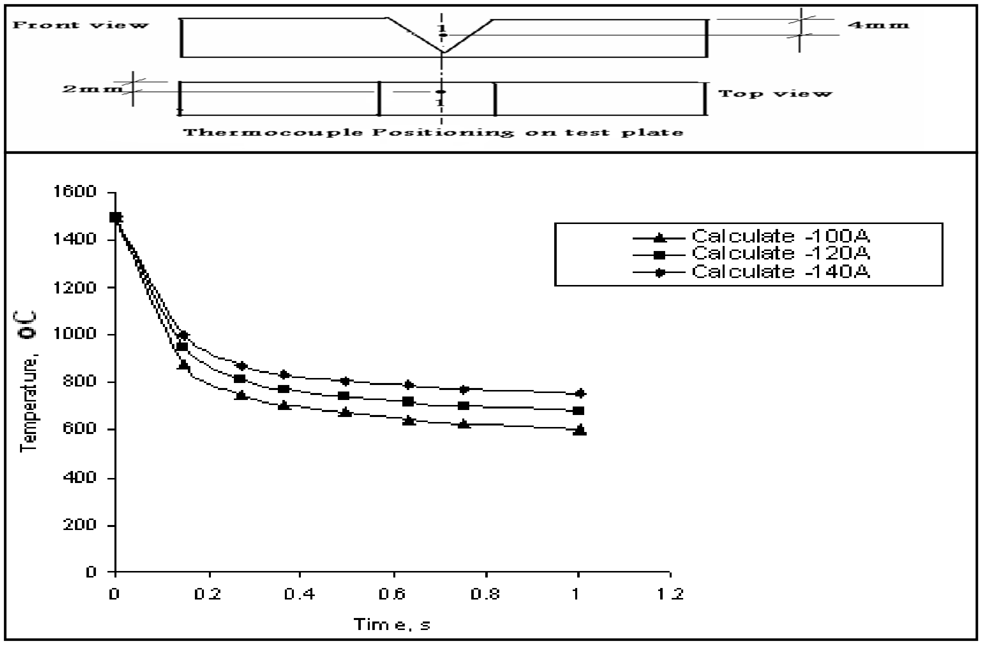

Figure (1) Single V- joint design of work pieces.

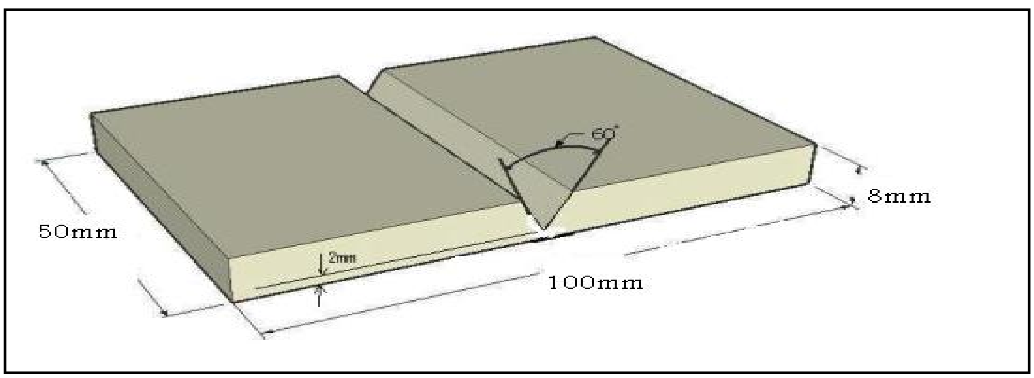

Figure (2) Experimental cooling curve at position fusion zone .Welding current 100A, 120A and 140A. Welding Speed 3.2 mm/sec and preheat temperature 100 C°.

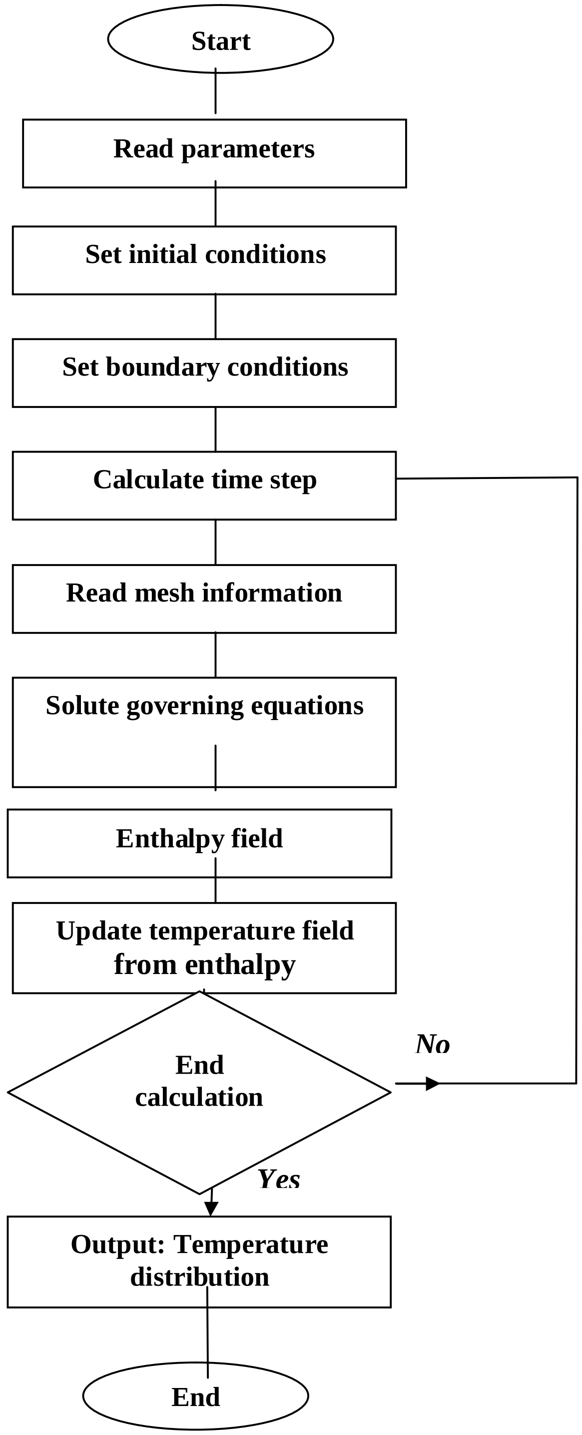

Figure (3) The computer flow chart by (CVM) program of welding process.

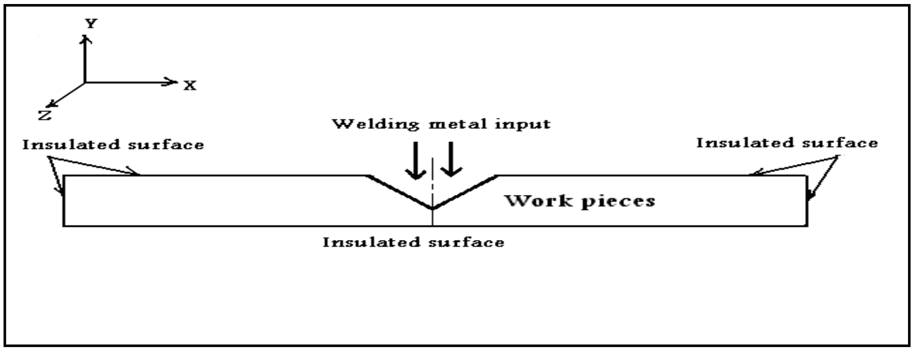

Figure (4) A schematic diagram of the boundary conditions used in this work

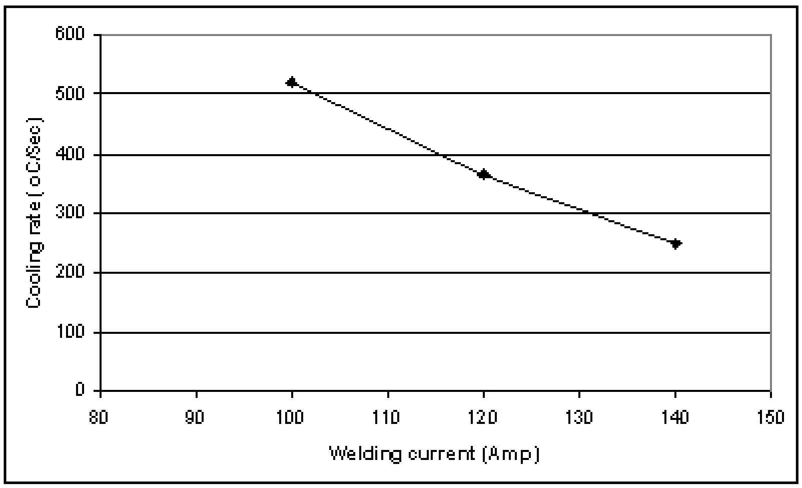

Figure (5) Relationship between welding current and cooling rate and at constant speed.

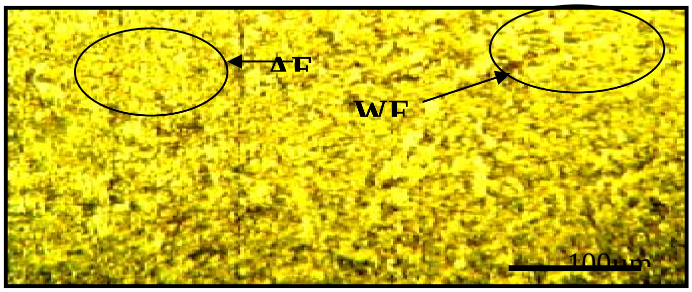

a-Weld metal region at weld current 100Amp

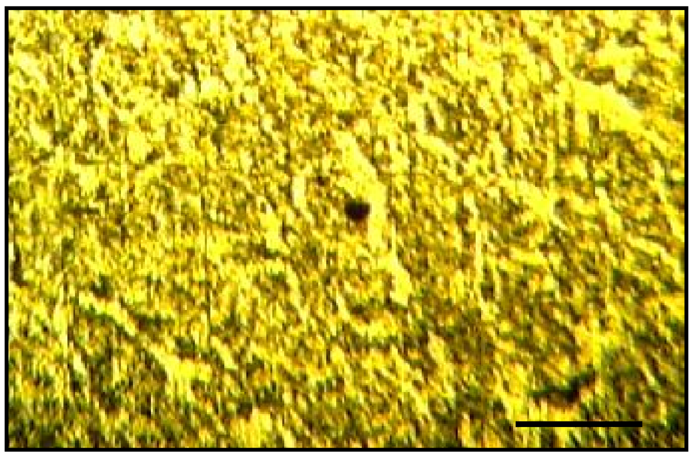

b-Weld metal region at weld current 120Amp

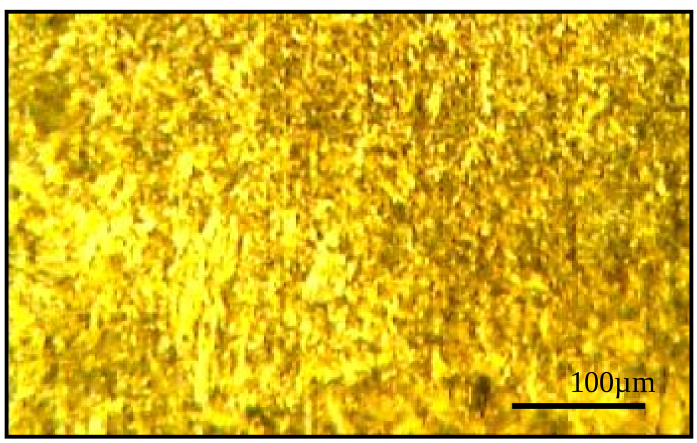

c-Weld metal region at weld current 140Amp

Figure (6) Microstructure of weld metal butt joint at different welding currents, preheat temp 100 ºC and electrode speed 3.2 mm / s.

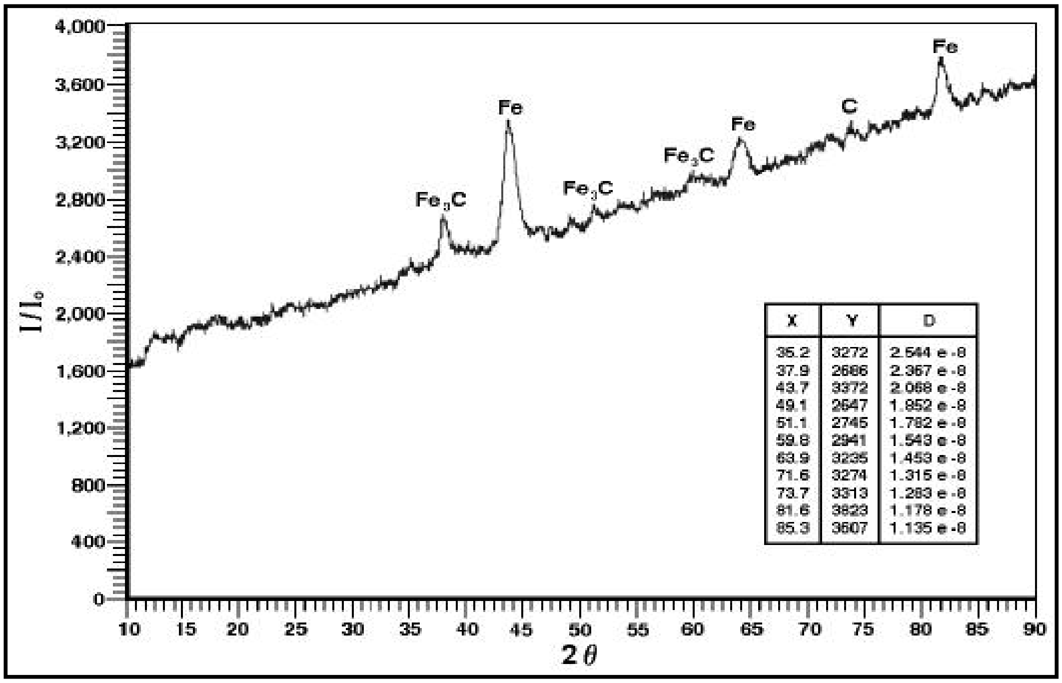

Figure (7) X – ray diffraction examination of weld metal joint C1.

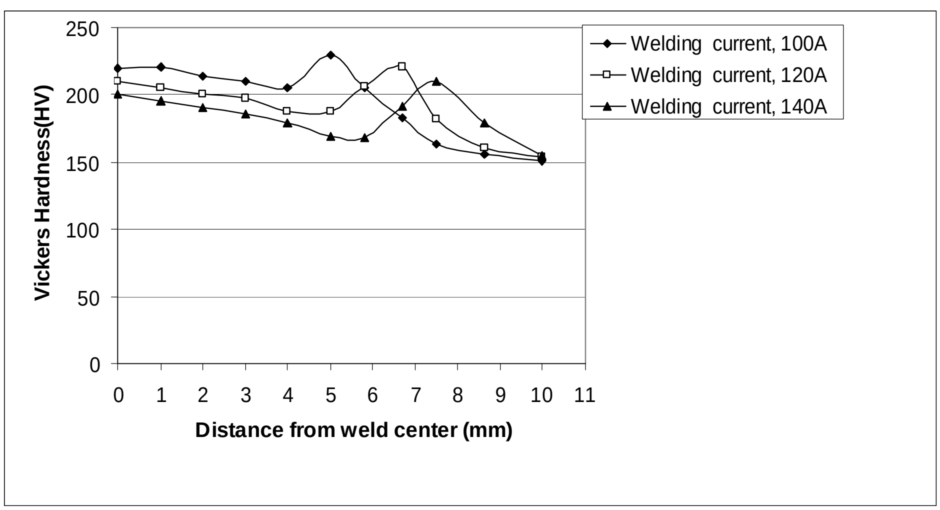

Figure (8) Effect of welding current on the micohardness at welding speed 3.2mm/s and preheat temperature 100°C.

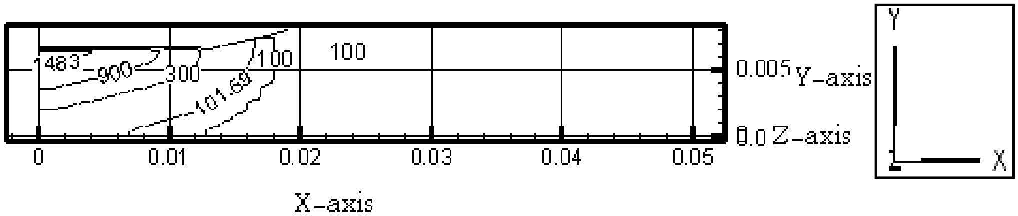

(a) 100A

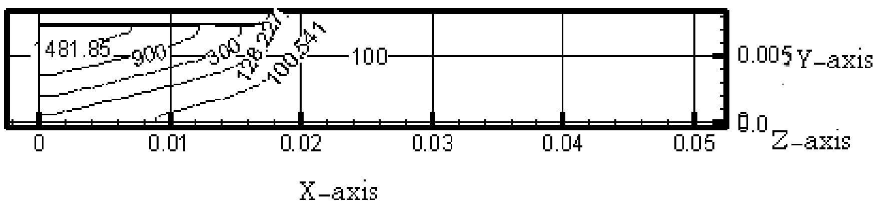

(b) 120A

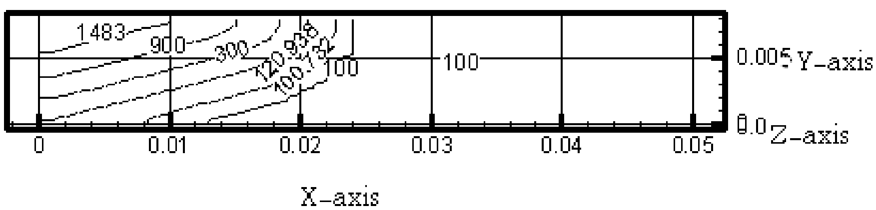

(c) 140A

Figure (9) Program temperature history at x=0 plane (welding speed 3.2mm/s, preheat temperature 100°C, time=0.1s at different welding current.

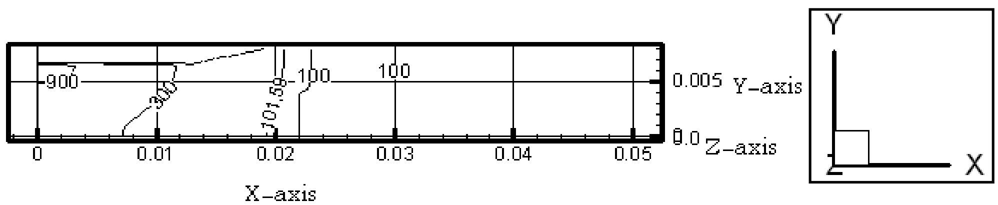

(a) 100A

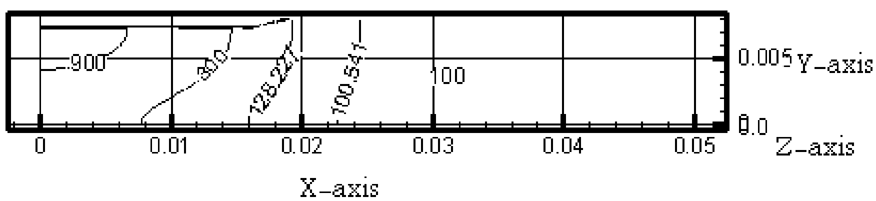

(b) 120A

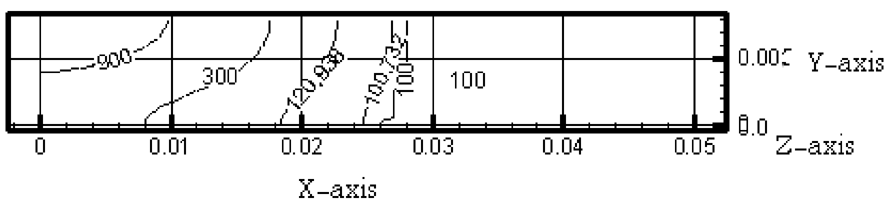

(c) 140A

Figure (10) Program temperature history at x=0 plane (welding speed 3.2mm/s, preheat temperature 100°C, time=0.5s at different welding current.

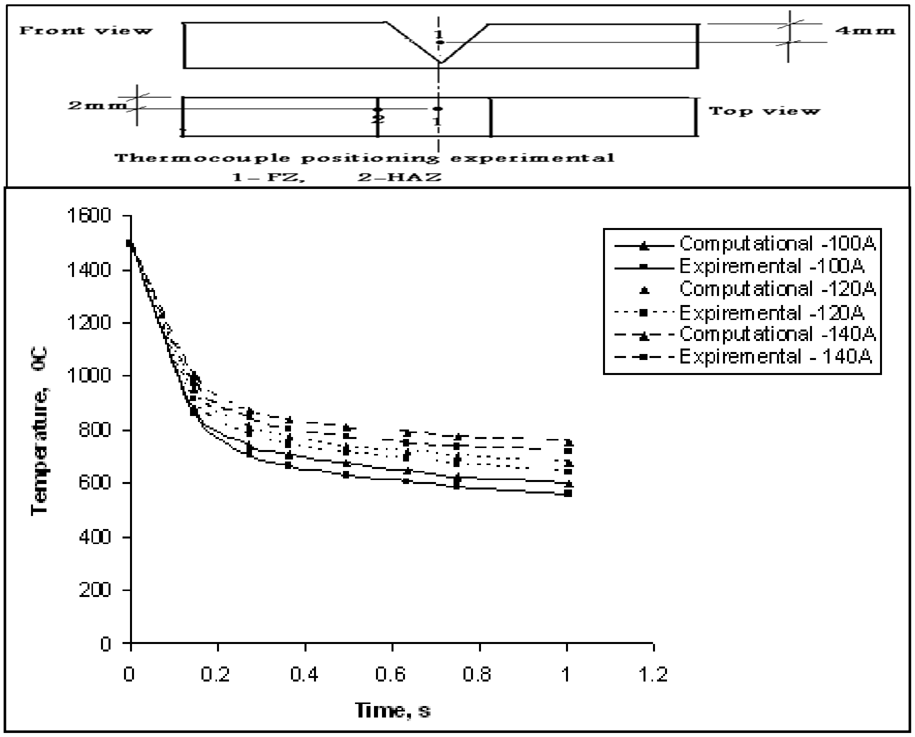

Figure (11) Comparison between computational and experimental results of cooling curves at fusion zone (FZ). Welding speed 3.2mm/s, preheat temperature 100°C, and different welding current.